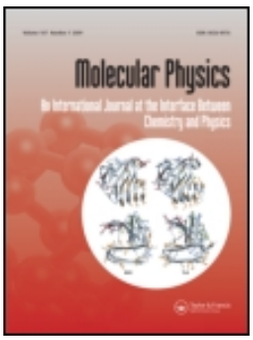

Molecular Physics

ISSN: 0026-8976 (Print) 1362-3028 (Online) Journal homepage: https://www.tandfonline.com/loi/tmph20

Long-time behaviour of quantized distributions in forward–backward semiclassical dynamics

J. Liu , A. Nakayama & N. Makri

To cite this article: J. Liu , A. Nakayama & N. Makri (2006) Long-time behaviour of quantized distributions in forward–backward semiclassical dynamics, Molecular Physics, 104:08, 1267-1274, DOI: 10.1080/00268970500525754

To link to this article: https://doi.org/10.1080/00268970500525754

Published online: 15 Dec 2010.

Molecular Physics, Vol. 104, No. 8, 20 April 2006, 1267–1274

Taylor & Francis
Taylor & Francis Group

Long-time behaviour of quantized distributions in forward–backward semiclassical dynamics

J. LIU, A. NAKAYAMA and N. MAKRI*
University of Illinois, Urbana, USA

(*Received 16 August 2005; in final form 20 October 2005*)

The paper reports investigations of the characteristics of phase space distributions in forward–backward semiclassical dynamics (FBSD) calculations. By virtue of Liouville's theorem and energy conservation, the volume of the negative regions is rigorously conserved and the energy distribution is invariant during time evolution. Thus, while the phase space density is not invariant under FBSD, exhibiting a weak time dependence mostly in its wings, it retains its quantum mechanical characteristics and does not revert to a classical Boltzmann distribution at long times. Illustrative applications on liquid neon near its triple point are presented.

1. Introduction

The forward–backward semiclassical dynamics (FBSD) methodology [1–7] has emerged as a rigorous, yet practical approximation to time-dependent quantum mechanical properties of condensed phase systems. Starting from the semiclassical phase space representation of a time-dependent observable or correlation function and performing a series of transformations, including the use of a derivative identity and the evaluation of the midpoint integral by the stationary phase method, FBSD expressions assume a quasiclassical form where the dynamical variables of interest are averaged with respect to a phase space distribution that corresponds to the quantized initial density. The main appeal of this expression is its simple form in terms of an integral over initial trajectory values, the absence of a rapidly oscillatory phase, and the feasibility of evaluating the particular phase space transform of the density operator without introducing additional approximations. The methodology also invites the use of molecular dynamics tools in the evaluation of the integrals [8] and can be combined with on-the-fly electronic structure techniques. The FBSD approximation may also be obtained as the stationary phase limit of the path integral representation to a time correlation function. As such, this particular (and most practical) version of FBSD cannot account for quantum interference effects that characterize low-dimensional molecular systems. Miller and co-workers have proposed expressions [9] that interpolate continuously between the more accurate (and less practical for polyatomic systems) semiclassical form and its full FBSD limit. Recent calculations [8, 10–13] have confirmed the ability of the quasiclassical FBSD methodology to capture important quantum effects, even dynamical effects associated with Bose–Einstein condensation [12, 13], and its suitability for simulations with hundreds of particles.

The FBSD approximation to a time correlation function corresponding to the inner product of two vector operators $\hat{\mathbf{A}}$ and $\hat{\mathbf{B}}$

$$C_{\mathbf{A}\cdot\mathbf{B}}(t) \equiv \mathrm{Tr}\Big(\hat{\rho}_0\hat{\mathbf{A}}\cdot e^{i\hat{H}t/\hbar}\hat{\mathbf{B}}e^{-i\hat{H}t/\hbar}\Big), \tag{1.1}$$

takes the form [7, 9, 14]

$$\begin{aligned} C^{\mathrm{FBSD}}_{\mathbf{A}\cdot\mathbf{B}}(t) = (2\pi\hbar)^{-n}\int d\mathbf{x}_0 d\mathbf{p}_0 \Big\{ \big(1+\tfrac{1}{2}n\big)\langle g_{\mathbf{x}_0\mathbf{p}_0}|\hat{\rho}_0\hat{\mathbf{A}}|g_{\mathbf{x}_0\mathbf{p}_0}\rangle \\ -2\langle g_{\mathbf{x}_0\mathbf{p}_0}|(\hat{\mathbf{x}}-\mathbf{x}_0)\cdot\boldsymbol{\Gamma}\hat{\rho}_0\hat{\mathbf{A}}\cdot(\hat{\mathbf{x}}-\mathbf{x}_0)|g_{\mathbf{x}_0\mathbf{p}_0}\rangle\Big\} \\ \times \mathbf{B}\big(\mathbf{x}_t,\mathbf{p}_t\big). \end{aligned} \tag{1.2}$$

Here n is the number of degrees of freedom in the system described by the coordinates x_j and momenta p_j, $j=1,\ldots,n$, $g_{\mathbf{x}_0\mathbf{p}_0}$ are coherent states with wavefunctions given by the relation

$$\begin{aligned} \langle \mathbf{x} \mid g_{\mathbf{x}_0\mathbf{p}_0}\rangle = \left(\frac{2}{\pi}\right)^{n/4}\det(\boldsymbol{\Gamma})^{1/4} \\ \times \exp\left(-(\mathbf{x}-\mathbf{x}_0)\cdot\boldsymbol{\Gamma}\cdot(\mathbf{x}-\mathbf{x}_0)+\frac{i}{\hbar}\mathbf{p}_0\cdot(\mathbf{x}-\mathbf{x}_0)\right) \end{aligned} \tag{1.3}$$

*Corresponding author. Email: nancy@makri.scs.uiuc.edu

Molecular Physics
ISSN 0026–8976 print/ISSN 1362–3028 online © 2006 Taylor & Francis
http://www.tandf.co.uk/journals
DOI: 10.1080/00268970500525754

(where $\mathbf{\Gamma}$ is the diagonal matrix of coherent state parameters γ_j), and $\mathbf{x}_t$, $\mathbf{p}_t$ are the phase space coordinates reached at the time t by a classical trajectory originating at $\mathbf{x}_0,\mathbf{p}_0$. Equation (1.2) is derived by expressing the operator $\hat{\mathbf{B}}$ in an exponential derivative form and applying the time-dependent semiclassical approximation in the coherent state representation [15] to the resulting product of exponential operators. Thus, the FBSD approximation is the stationary phase limit of a Heisenberg-evolved operator expressed in an exponential form.

To implement the approximation, classical trajectories are sampled from a phase space distribution given by the absolute value of the exponential part of

$$\mathscr{P}_A(\mathbf{x}_0,\mathbf{p}_0;0) = \left\langle g_{\mathbf{x}_0,\mathbf{p}_0}\middle|\left(1+\tfrac{1}{2}n\right)\hat{\rho}_0\hat{A} - 2(\hat{\mathbf{x}}-\mathbf{x}_0)\cdot\mathbf{\Gamma}\hat{\rho}_0\hat{A}\cdot(\hat{\mathbf{x}}-\mathbf{x}_0)\middle|g_{\mathbf{x}_0,\mathbf{p}_0}\right\rangle. \quad (1.4)$$

Because this operator involves only equilibrium properties, it can be fully quantized (e.g. by expressing the Boltzmann operator as an imaginary time path integral [16]). The accurate representation of the phase space distribution that determines the weights of the classical trajectories ensures a correct description of important quantum mechanical effects associated with zero-point energy, frequency shifts, and imaginary components that are responsible for spectral asymmetries. At the same time, the combination of a quantum mechanical treatment of the initial density with a subsequent classical propagation leads to various inconsistencies. Among the most significant questions that arise are (i) whether FBSD obeys certain relations satisfied by exact quantum mechanical correlation functions, and (ii) how the quantized distribution evolves at long times. The first of these questions was addressed in a recent paper [17], where we showed that autocorrelation functions satisfy rigorously an important time symmetry and the related detailed balance condition. The characteristics of the long-time evolution of the quantized phase space density are the subject of the present work.

If $\hat{A}=1$ in the correlation function, then equation (1.2) gives the expectation value for the operator $\hat{B}$ during the time evolution, and equation (1.4) provides the FBSD corresponding phase distribution function for the density operator $\hat{\rho}_0$. In FBSD, the combination of a quantum mechanical treatment of the initial density with a subsequent classical propagation leads to various inconsistencies. As the quantized phase space density is not steady under classical dynamics, and a large system (condensed phase system) usually is in practice ergodic, one might expect it will show classical mechanical relaxation behavior and finally reach an 'equilibrium' state characterized by a classical Boltzmann-like distribution at some effective temperature. In the next two sections we show that this is not the case, although the evolving distribution does deviate from the correct quantum mechanical density, retaining important quantum mechanical structures as it develops certain classical-like features.

In the next section, we investigate various general properties of the phase space density evolving according to the FBSD approximation. In section 3, we illustrate these properties with a simulation on liquid neon and examine the long-time characteristics of this density, and section 4 concludes.

2. Theoretical analysis

Using the path integral representation of the Boltzmann operator $\hat{\rho}_0 = \exp(-\beta\hat{H})/Z$ (where Z is the canonical partition function), the FBSD expression for a thermal correlation function takes the form [6]

$$C_{\mathbf{A}\cdot\mathbf{B}}(t) = (2\pi\hbar)^{-n}\int d\mathbf{x}_0\int d\mathbf{p}_0\int d\mathbf{x}_1\cdots\int d\mathbf{x}_N \Theta(\mathbf{x}_0,\mathbf{p}_0,\mathbf{x}_1,\ldots,\mathbf{x}_N)\Lambda_{\mathbf{A}\cdot\mathbf{B}}(\mathbf{x}_0,\mathbf{p}_0,\mathbf{x}_1,\ldots,\mathbf{x}_N). \quad (2.1)$$

Here, $\mathbf{x}_1,\ldots,\mathbf{x}_N$ are the N auxiliary path integral variables (the 'beads') that arise from splitting the Boltzmann operator into N factors corresponding to imaginary time $\Delta\beta=\beta/N$, each of which is factored using the Trotter approximation,

$$\begin{aligned}
&\Theta(\mathbf{x}_0,\mathbf{p}_0,\mathbf{x}_1,\ldots,\mathbf{x}_N)\\
&= \left\langle g_{\mathbf{x}_0,\mathbf{p}_0}\middle|e^{-\Delta\beta\hat{H}_0/2}|\mathbf{x}_1\rangle e^{-\Delta\beta V(\mathbf{x}_1)}\langle\mathbf{x}_1|e^{-\Delta\beta\hat{H}_0}|\mathbf{x}_2\rangle\ldots\right.\\
&\quad\left.\times e^{-\Delta\beta V(\mathbf{x}_N)}\langle\mathbf{x}_N|e^{-\Delta\beta\hat{H}_0/2}\middle|g_{\mathbf{x}_0,\mathbf{p}_0}\right\rangle\\
&= \prod_{j=1}^{n}\left(\frac{2\gamma_j}{\pi}\right)^{1/2}\frac{m_j}{m_j+\hbar^2\Delta\beta\,\gamma_j}\left(\frac{m_j}{2\pi\hbar^2\Delta\beta}\right)^{(N-1)/2}\\
&\quad\times\exp\left\{-\frac{m_j}{m_j+\hbar^2\Delta\beta\,\gamma_j}\left(\gamma_j(x_{j,1}-x_{j,0})^2+\gamma_j(x_{j,N}-x_{j,0})^2\right.\right.\\
&\qquad\left.+\frac{\Delta\beta}{2m}p_{j,0}^2+\frac{i}{\hbar}p_{j,0}(x_{j,1}-x_{j,N})\right)\\
&\qquad\left.-\frac{m_j}{2\hbar^2\Delta\beta}\sum_{k=2}^{N}\left(x_{j,k}-x_{j,k-1}\right)^2-\Delta\beta\sum_{k=1}^{N}V(x_{j,k})\right\}
\end{aligned} \quad (2.2)$$

is the path integral discretization of the coherent state transform of the Boltzmann operator alone, m_j is the mass associated with the jth degree of freedom,

and the function $\Lambda_{\mathbf{A}\cdot\mathbf{B}}$ depends on the specific form of the operators.

Because FBSD propagates each phase space point by classical mechanics, the time evolution of the phase distribution is governed by Liouville's theorem, which states that

$$\frac{\partial \mathscr{P}_A}{\partial t} = -\{\mathscr{P}_A, H\} = -\frac{\partial \mathscr{P}_A}{\partial \mathbf{x}} \cdot \frac{\partial H}{\partial \mathbf{p}} + \frac{\partial \mathscr{P}_A}{\partial \mathbf{p}} \cdot \frac{\partial H}{\partial \mathbf{x}}$$

$$= -\frac{\partial \mathscr{P}_A}{\partial \mathbf{x}} \cdot \frac{\mathbf{p}}{m} + \frac{\partial \mathscr{P}_A}{\partial \mathbf{p}} \cdot \frac{\partial V(\mathbf{x})}{\partial \mathbf{x}}. \tag{2.3}$$

In the Langrangian view, where properties are examined along the flow, the phase distribution function is invariant during the evolution, i.e.

$$\mathscr{P}_A(\mathbf{x}_t, \mathbf{p}_t; t) = \mathscr{P}_A(\mathbf{x}_0, \mathbf{p}_0; 0) \tag{2.4}$$

By virtue of this fact, even though the phase distribution in the Euler representation may change or distort from its initial form, the total volume of its negative regions is a time-invariant property.

For $\hat{A} = 1$ in the correlation function, equation (1.4) provides the FBSD phase space distribution $\mathscr{P}_{A=1}(\mathbf{x_0}, \mathbf{p_0})$ for the initial density operator. This distribution, in turn, determines the energy distribution,

$$f(E) = \int \mathbf{dx}_0 \int \mathbf{dp}_0 \, \mathscr{P}_{A=1}(\mathbf{x_0}, \mathbf{p_0}) \, \delta\big(E - H(\mathbf{x_0}, \mathbf{p_0})\big). \tag{2.5}$$

Since the energy is conserved along each classical trajectory employed in FBSD, the energy distribution $f(E)$ will not change during the evolution. As each trajectory reaches its micro-canonical equilibrium state in an ergodic system, the entire distribution will reach its equilibrium state as well, which means its thermodynamic properties attain constant values. The final phase distribution of such an ergodic large system will depend on $f(E)$ only, and thus is steady (time-invariant) under the classical dynamics. In other words, the density phase distribution at the equilibrium in the FBSD approximation is given by

$$\mathscr{P}_{\text{eq}}(\mathbf{x}, \mathbf{p}) = \mathscr{P}_{A=1}(\mathbf{x}, \mathbf{p}; t \to \infty) = f(E = H(\mathbf{x}, \mathbf{p})). \tag{2.6}$$

The equilibrium phase space distribution $\mathscr{P}_{A=1}(\mathbf{x}, \mathbf{p}; t)$ is totally determined by the quantization $\mathscr{P}_{A=1}(\mathbf{x_0}, \mathbf{p_0})$ of the density operator. Thus the coherent state width may show its weak influence on $\mathscr{P}_{\text{eq}}(\mathbf{x}, \mathbf{p})$. As a result of this quantization, the phase space distribution $\mathscr{P}_{A=1}(\mathbf{x_0}, \mathbf{p_0})$ and thus the energy distribution $f(E)$ has both positive and negative regions. Hence the final distribution $\mathscr{P}_{\text{eq}}(\mathbf{x}, \mathbf{p})$ will be different from the classical Boltzmann distribution in phase space, retaining important structures associated with quantization rather than relaxing to a pure classical distribution as it reaches equilibrium. Another characteristic property is the momentum distribution,

$$\sigma(\mathbf{p}; t) = \int \mathbf{dx} \, \mathscr{P}_{A=1}(\mathbf{x}, \mathbf{p}; t) \tag{2.7}$$

This function will also have positive and negative regions. Therefore, the long-time 'equilibrium' momentum distribution in the FBSD approximation differs from the Maxwell–Boltzmann distribution. In the next section we retain the use of the relation $\langle \mathbf{p}^2/2m \rangle = \frac{3}{2} k_B T$ to infer the 'equilibrium temperature' of the system after a long-time relaxation of its initial quantized phase space distribution, but it should be clear that the FBSD density never changes to that charactering classical mechanical systems.

For each constant energy surface of the phase space distribution, phase space points carrying initially positive and negative weights will mix as time progresses, showing a similar behavior as described in a one-dimensional system in a previous paper [18]. Finally, in the high-temperature limit, the quantized phase space density distribution will reduce to its corresponding classical Boltzmann distribution, and hence the phase distribution function will be time-invariant.

3. Numerical illustrations

In this section we illustrate the phase space characteristics and long-time limit of FBSD with a simulation on liquid neon. While fully quantum mechanical results on liquids are not available for comparison, several tests on model systems have shown the FBSD methodology to give nearly quantitative results (as long as quantum interference effects are not significant). We choose $\mathbf{\Gamma} = \gamma \mathbf{1}$, where $\mathbf{1}$ is the identity matrix. The system is treated as a Lennard–Jones fluid with parameters $\sigma = 2.749\,\text{Å}$, $\varepsilon/k_B = 35.6\,\text{K}$ and $m = 3.35 \times 10^{-26}\text{kg}$, at a reduced density $\rho^* = 0.78$ and reduced temperature $T^* = 0.84$. This state point is at a fairly low temperature ($T = 29.9\text{K}$), while still in the liquid region of both the Lennard–Jones and experimental phase diagrams [11, 19, 20]. Quantum effects are significant under these conditions: the kinetic energy computed by path integral Monte Carlo methods is 55.15 K, amounting to a 20% quantum correction to the classical kinetic energy of 44.85 K. These sizable quantum mechanical effects arise from the large zero-point energy of the light neon atoms. The dynamical consequences of these quantum effects are even greater: the momentum autocorrelation function computed by FBSD was found to differ substantially from that obtained by classical molecular

dynamics methods, and various quantum correction factor prescriptions give rise to different results, none of which are in perfect agreement with the FBSD results [11]. Using the pair-product (PP) approximation [10] to the coherent state matrix element of the Boltzmann operator, the present simulation converged with a single path integral bead.

First, we investigate the expectation value of the kinetic energy by setting $\hat{A} = 1$, $\hat{B} = \hat{\mathbf{p}}^2/2m$. As discussed in earlier work [18], FBSD averages evaluated with this choice of operators depend sensitively on the wings of the phase space distribution, leading to poor Monte Carlo statistics. Although FBSD methodology is in principle exact at zero time, we were unable to converge the FBSD results for the average kinetic energy of liquid neon to better than 5%. We find, however, that the change with time of the system's kinetic energy relative to its initial value is well-converged in our calculation. For this purpose we display in figure 1 corrected average kinetic energy values, which we obtained by shifting the simulation results by the amount necessary to make the initial value equal to that obtained from a high-precision PIMC calculation (2.64 K for $\gamma = 6$ a.u., 2.66 K for $\gamma = 8$ a.u.).

Figure 1 shows the time evolution of the system's average kinetic energy per molecule for two near-optimal values of the coherent state parameter. It is seen that the average kinetic energy approaches a nearly constant value following an initial time interval of approximately 0.7 ps, during which the kinetic energy changes nonmonotonically. The spurious variation of the liquid's kinetic energy is a consequence of the non-commutation between the quantum mechanical treatment of the Boltzmann operator and the classical Liouville operator generating the time evolution of this density. As seen in figure 1, the difference of the initial (55.15 K) and equilibrium (about 50 K) values depends weakly on the coherent state width. Although the average kinetic energy decreases by about 5 K during the course of FBSD time evolution, its final value remains well above the corresponding classical value. For comparison, the temperature at which the quantum mechanical expectation value of the system's kinetic energy (obtained by PIMC) at the same density ($\rho^* = 0.78$) is 50 K (i.e. equal to the FBSD long-time value) is $T = 26.19$ K.

Before proceeding with further analysis of these simulation results, we show in figure 2 a snapshot of the atomic positions (coordinates of the coherent state centers) and PP-path integral coordinates (beads) at the final equilibrium state reached by one of the FBSD trajectories. The observed randomness suggests that the system is still in a typical liquid configuration (although at a lower temperature) and has not phase-separated.

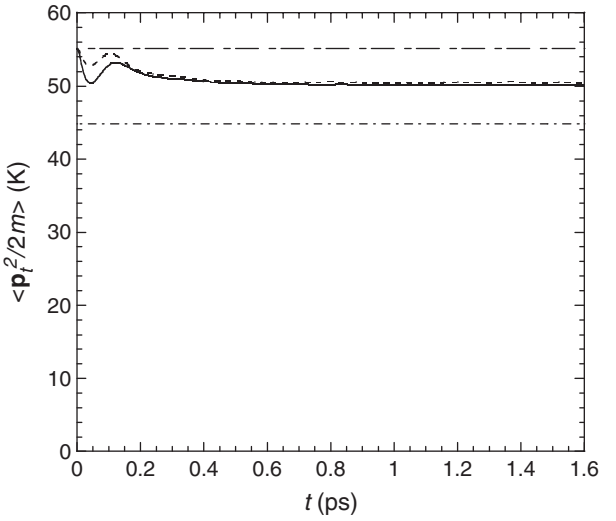

Figure 1. Evolution of the average system kinetic energy $\langle \mathbf{p}_t^2 \rangle / 2m$. Solid line: $\gamma = 6$ a.u. Dashed line: $\gamma = 8$ a.u. Chain-dashed line: quantum mechanical result. Chain-dotted line: classical mechanical result.

The time dependence in the expectation value of the kinetic energy (in principle, a conserved quantity) observed in figure 1 is at first disturbing. In a recent paper we investigated various theoretical features of FBSD expressions and showed that an important time symmetry, which is responsible for the detailed balance relation, is satisfied rigorously in the FBSD methodology only for time *auto*correlation functions. In view of this property, the non-stationarity of expectation values is not surprising. In a certain sense, the higher symmetry attained in expressions where the two operators are identical alleviates some of the inconsistency caused in FBSD by the classical mechanical propagation of an initially quantized phase space distribution.

Figure 3 shows FBSD results with $\hat{A} = \hat{\mathbf{p}}$, $\hat{B} = \hat{\mathbf{p}}/2m$ for liquid neon under the same conditions. This quantity is proportional to the system's velocity autocorrelation function (although the normalization is chosen such that at zero time the real part of figure 3 coincides with that in figure 1). Not only do the results shown in figure 3 exhibit a negligible dependence on the coherent state width within the chosen range, they also converge much better than those for the average kinetic energy shown in figure 1 (and thus appear as a smoother curves).

To shed more light on the characteristics of the evolving phase space distribution, we calculate the pair distribution function $g(r)$ using

$$\hat{A} = 1, \quad \hat{B} = \frac{v}{n_{\mathrm{p}}^2} \sum_{i<j}^{n_{\mathrm{p}}} \delta\left(r - |\hat{\mathbf{r}}^{(i)} - \hat{\mathbf{r}}^{(j)}|\right) \qquad (3.1)$$

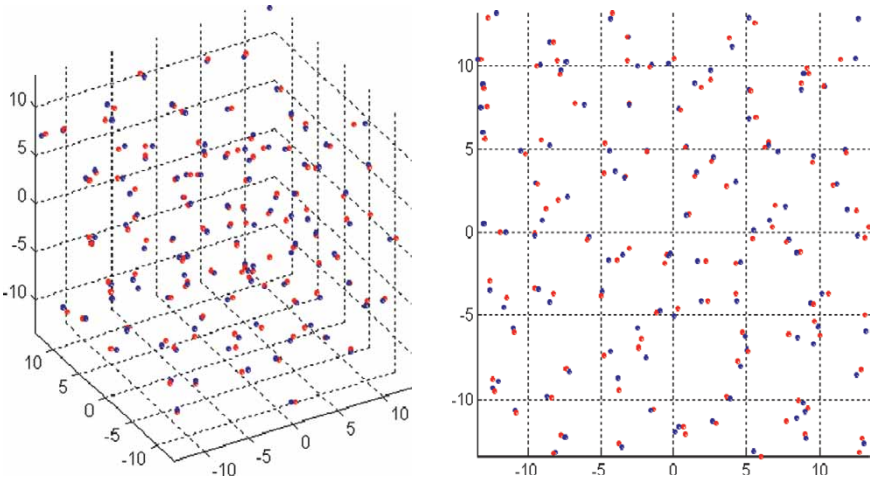

Figure 2. Final three-dimensional configuration of the neon system through FBSD and its two-dimensional projection. The simulation employed 108 atoms in the unit cell with periodic boundary conditions. The coordinates of each atom are shown in red, and the PP bead is shown in blue.

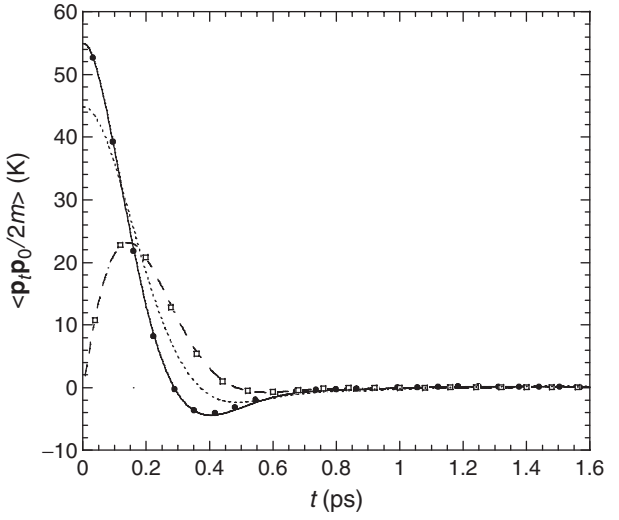

Figure 3. Autocorrelation function $\langle \mathbf{p}_0 \cdot \mathbf{p}_t \rangle / 2m$, where γ is the width parameter of the coherent state. Solid line: real part of the correlation function with $\gamma = 6$ a.u. Long-dashed line: imaginary part of the correlation function with $\gamma = 6$ a.u. Solid circles: real part of the correlation function with $\gamma = 8$ a.u. Hollow squares: imaginary part of the correlation function with $\gamma = 8$ a.u. Short-dashed line: classical molecular dynamics results.

where n_p is the number of particles in the box of the simulation, and the molar volume $v = 16.04\ \mathrm{cm^3\,mol^{-1}}$. Below we compare the pair distribution function obtained at select times during the FBSD evolution with the corresponding quantum mechanical and classical results.

Figure 4 shows the pair distribution function at different times during the evolution. Time $t = 0$ represents the initial pair distribution function, $t = 0.048$ ps corresponds to the time at which the system kinetic energy is at its first local minimum in figure 1, $t = 0.133$ ps is the time at the peak in figure 1, and $t = 1.004$ ps and $t = 1.604$ ps are times at which the system kinetic energy has attained its equilibrium value. The height of the first peak of the pair distribution function decreases at the beginning until the system kinetic energy reaches its peak in figure 1, and then increases until it reaches its final value. During the course of classical mechanical propagation in FBSD, the initially quantized phase space density changes in complex ways that at short times appear to combine both classical and quantum mechanical features. Thus, in spite of a sharp decrease in the average kinetic energy at $t = 0.048$ ps (which is typical of evolution toward a classical-like density), the first peak in the pair distribution function appears at that time slightly lowered (a characteristic of a quantum mechanical trend). The first peak of the distribution function is further lowered considerably at $t = 0.133$ ps, when the average kinetic energy goes through a local maximum. Eventually, at long times, the peak in $g(r)$ recovers its original height, although its position has moved to a slightly shorter interatomic distance.

Figure 5 shows the initial and final pair distribution functions in the FBSD calculation, and also their quantum mechanical and classical counterparts at $T = 29.90$ K and $T = 26.19$ K. The second of these temperatures is that at which the quantum mechanical kinetic energy of the system equals that attained at long times by the FBSD-evolved density. As shown in figure 4, the first peak occurs at an interatomic distance smaller than the position of the Lennard–Jones potential minimum $r_{\min} = \sqrt[6]{2}\sigma = 3.0856$ Å for liquid neon. At the initial point $t = 0$ ps ($T = 29.90$ K), using the

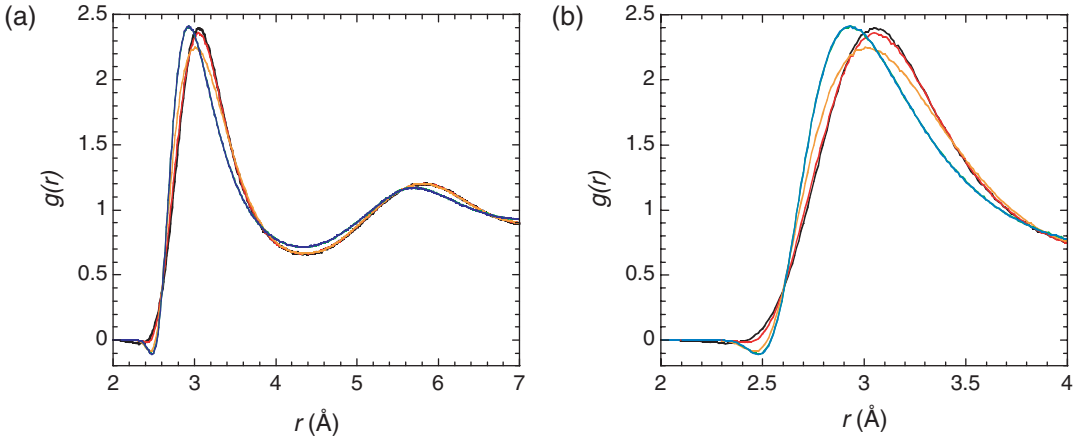

Figure 4. Evolution of the pair distribution function $g(r)$ with $\gamma = 6$ a.u. Black line: $t = 0$ ps. Red line: $t = 0.048$ ps. Orange line: $t = 0.133$ ps. Green line: $t = 1.0038$ ps. Blue line: $t = 1.604$ ps. (The green and blue lines essentially coincide). Panel (b) shows a blowup of the curves shown in (a).

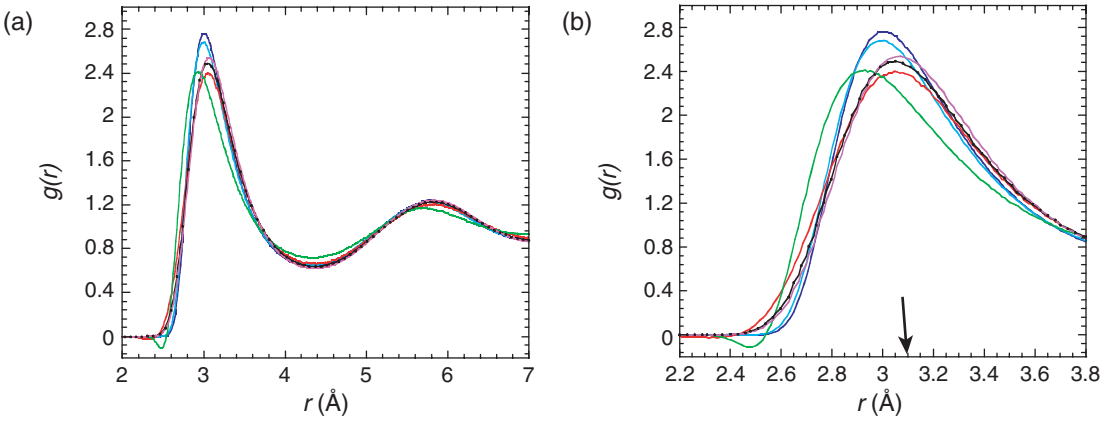

Figure 5. Comparison of the initial and final pair distribution functions $g(r)$ to their quantum mechanical (PIMC) and classical mechanical (CMC) counterparts. The coherent state width parameter in the FBSD calculations is $\gamma = 6$ a.u. Cyan line: CMC at $T = 29.90$ K. Blue line: CMC at $T = 26.19$ K. Red line: PP-FBSD at $t = 0$ ps. Green line: FBSD at $t = 1.604$ ps. Black line and circles: PIMC at $T = 29.90$ K. Purple line: PIMC at $T = 26.19$ K. The arrow shows the position of the minimum of the Lennard–Jones potential $r_{\min}$. Panel (b) shows a blowup of the curves shown in (a).

PP approximation to the coherent state matrix element of the Boltzmann operator with only one bead, the FBSD simulation results (the position and height of the first peak of the pair distribution function) are in reasonable agreement with the results of a path integral Monte Carlo (PIMC) simulation (which required up to 20 beads for convergence). The small (3.71 K) drop of the system temperature causes the first peak of the pair distribution function in the PIMC or CMC calculations to move very slightly to the right. This is so because a decrease in temperature implies a decrease in the system's kinetic and potential energy for the quantum mechanical and classical simulations; since the first peak of the pair distribution function lies on the left of the potential minimum, a decrease in potential energy leads to right shift in the peak of $g(r)$. By contrast, the first peak of the final pair distribution function in the FBSD calculation exhibits a noticeable shift to the left of its initial value. The pair distribution function obtained with $\gamma = 8$ a.u. exhibits similar trends. In the FBSD simulation, the system kinetic energy is lowered relative to its initial value as shown in figure 1, but since the propagation conserves the total energy, the average potential energy must increase as the final 'equilibrium' state is reached, leading to the observed shift of the peak toward a shorter interatomic distance. Similar arguments apply to the second peak of the pair distribution function.

The shift of the peak in the pair distribution function in figures 4 and 5, along with the relaxation behaviour shown in figure 1, clearly illustrates that time evolution under FBSD does not preserve the exact shape of the phase space density. This artifact is a result of the inconsistent treatment of the initial density (which is fully quantized) and its time evolution (which is obtained from classical trajectories). Furthermore, one concludes from figure 5 that the 'equilibrium' state reached by FBSD matches neither the quantum mechanical nor the classical phase space distributions at either the actual or the final FBSD temperatures. Though this 108-atom simulation shows ergotic behavior under classical dynamics, the FBSD final 'equilibrium' is *not* a classical Boltzmann distribution for a system in a different thermodynamic state. In this sense, one should not, strictly speaking, extract a 'temperature' from the FBSD kinetic energy (except at zero time). As we discussed in the previous section, classical dynamics preserves the volume of negative parts of the phase space density distribution, therefore the FBSD phase space density will under no circumstances evolve into a (positive definite) classical Boltzmann distribution.

4. Concluding remarks

We have examined the time evolution of the phase space density in FBSD, with emphasis on its long-time 'equilibrium' limit. Based on rigorous arguments, we have shown that the long-time phase space distribution retains important quantum mechanical structures built in its initial condition. As the energy distribution determined by the initial quantized density phase distribution is time invariant during the evolution, phase points of positive and negative density at the same energy may mix during propagation. By virtue of the Liouville's theorem, the volume of the negative regions is rigorously conserved, and so are the positive parts. As a consequence of these facts, the phase space distribution cannot revert to a classical Boltzmann distribution. At the same time, the classical propagation of each phase space point prevents stationarity, leading to a weak time-dependence of the evolving density.

Numerical simulations on liquid neon show that expectation values are harder to converge than time autocorrelation functions (which, as discussed in previous work [17], satisfy important properties), and that they exhibit a spurious time dependence that depends weakly on the coherent state width. Calculations of the pair distribution function show that the liquid retains a similar, but not identical structure to that corresponding to its initial quantized equilibrium state, which corresponds to a slightly decreased kinetic energy.

In recent years, much attention has been given to the Wigner quasiclassical (or linearized semiclassical initial value representation) approximation [21–25]. This is similar in structure to the FBSD expression, but the required numerical evaluation of the Wigner transform usually is feasible only with additional approximations. The theoretical analysis presented in this paper also applies to the Wigner approximation.

Acknowledgements

This material is based upon work supported by the US Department of Energy, Division of Materials Sciences under Award No. DEFG02-91ER45439, through the Frederick Seitz Materials Research Laboratory at the University of Illinois at Urbana-Champaign, and by the National Science Foundation Information Technologies Research program under Award No. NSF CHE 04-27082.

References

[1] N. Makri and K. Thompson, Chem. Phys. Lett. **291,** 101 (1998).
[2] K. Thompson and N. Makri, J. Chem. Phys. **110,** 1343 (1999).
[3] J. Shao and N. Makri, J. Phys. Chem. **103,** 7753 (1999).
[4] J. Shao and N. Makri, J. Phys. Chem. **103,** 9479 (1999).
[5] E. Jezek and N. Makri, J. Phys. Chem. **105,** 2851 (2001).
[6] N. Makri, J. Phys. Chem. **106,** 8390 (2002).
[7] N. Makri, A. Nakayama, and N. Wright, J. Theor. Computat. Chem. **3,** 391 (2004).
[8] N. J. Wright and N. Makri, J. Chem. Phys. **119,** 1634 (2003).
[9] M. Thoss, H. Wang, and W. H. Miller, J. Chem. Phys. **114,** 9220 (2001).
[10] A. Nakayama and N. Makri, J. Chem. Phys. **119,** 8592 (2003).
[11] C. P. Lawrence, A. Nakayama, N. Makri, and J. L. Skinner, J. Chem. Phys. **120,** 6621 (2004).
[12] A. Nakayama and N. Makri, Chem. Phys. **304,** 147 (2004).
[13] A. Nakayama and N. Makri, Proc. Natl. Acad. Sci. USA **102,** 4230 (2005).
[14] N. Makri and J. Shao, in *Accurate Description of Low-lying Electronic States and Potential Energy Surfaces*, edited by M. Hoffmann (Oxford University Press, 2002).
[15] M. F. Herman and E. Kluk, Chem. Phys. **91,** 27 (1984).
[16] R. P. Feynman, *Statistical Mechanics* (Addison-Wesley, Redwood City, 1972).
[17] J. Liu and N. Makri, Chem. Phys. (submitted).
[18] N. J. Wright and N. Makri, J. Phys. Chem. **108,** 6816 (2004).

[19] A. Rabinovich, A. A. Vasserman, V. I. Nedostup, and L. S. Veksler (Eds), Thermodynamic Properties of Neon, Argon, Krypton, and Xenon (Springer-Verlag, Berlin, 1988).
[20] J. K. Johnson, J. A. Zollweg, and K. E. Gubbins, Mol. Phys. **78,** 591 (1993).
[21] E. J. Wigner, Chem. Phys. **5,** 720 (1937).
[22] E. J. Heller, J. Chem. Phys. **65,** 1289 (1976).
[23] H. Wang, X. Sun, and W. H. Miller, J. Chem. Phys. **108,** 9726 (1998).
[24] Q. Shi and E. Geva, J. Phys. Chem. **107,** 9059 (2003).
[25] J. A. Poulsen, G. Nyman, and P. J. Rossky, J. Chem. Phys. **119,** 12179 (2003).